HEATING AND DECAY OF PLASMA PRODUCED BY A GIANT LASER PULSE FOCUSED ON A SOLID TARGET

N. G. BASOV, V. A. BOĬKO, V. A. DEMENT'EV, O. N. KROKHIN, and G. V. SKLIZKOV

P. N. Lebedev Physics Institute, Academy of Sciences, U.S.S.R.

Submitted to JETP editor March 21, 1966

J. Exptl. Theoret. Phys. (U.S.S.R.) 51, 989-1000 (October, 1966)

The process of formation and properties of a plasma ("flare") produced by a giant laser pulse focused on a solid target surface has been investigated. Space-time diagrams of the outward motion of the edge and various internal regions of the flare have been obtained. The distribution of particle concentration in the flare has been estimated and plasma mass and temperature have been measured as functions of the laser output power.

RECENT experimental research on the interaction of a giant laser pulse focused on a solid target has shown that plasma formed in the focus ("flare") can be heated in a short time to a temperature exceeding 10^5 degrees. A number of papers[1-6] presented a feasibility analysis of high-temperature plasma heating for the purpose of observing thermonuclear reactions. Such plasma can also be used to produce plasmoids of high chemical purity and to generate heavy pulsed currents of ions and electrons.[5-10]

Papers[8,10,7] presented flare temperature estimates based on the velocity of the ions emitted from the plasma surface. Haught and Polk[5] observed ions with energies of 300 and 2500 eV at laser powers of 20 and 500 megawatts respectively. Since their measurements were carried out at large distances, they failed to yield information on the distribution of gas-dynamic quantities in the flare in the initial stage of decay. In spite of the presence of ions with energies of the order of 1000 eV generated in the flare, there are indications that its temperature is much lower. The temperature of a flare formed on a lithium target has been estimated spectroscopically in[11]; the measured temperature was 10—20 eV for a power of 100 megawatts. Linlor[7] measured radiation absorption in a plasma produced by focusing laser emission on a thin metal foil and concluded that the coefficient of absorption must be high, since 99% of the incident radiation was absorbed at a total of $\sim 4 \times 10^{15}$ particles.

The present paper deals with an attempt to find a distribution of the basic gas-dynamic parameters of the flare during the early decay stages. For this purpose, experimental equipment with a high time resolution was used, allowing us to determine the radii of various regions of the flare as a function of time (R − t diagrams).

GAS-DYNAMIC MOTION OF THE FLARE

Papers dealing with the heating of matter by focusing intense laser emission on solid targets usually take gas-dynamic motion into account by using quantities averaged with respect to the gas mass.[1,4,5] The outward gas-dynamic motion of a given transparent heated gas mass has also been discussed in[12]. While in all these cases the gas mass was considered constant, in the experiments it increased as a rule because of heating. It would be of interest, therefore, to account for this phenomenon in the consideration of the gas dynamic motion of the flare.

Since such a problem can be solved only by numerical methods, it is appropriate to consider an approximate model that admits of an analytical solution. In the first approximation we assume spherical symmetry and solutions with a velocity linear in the radius (class of Sedov's solutions[13]), viz., $u = \dot{R}r/R$, where $\dot{R}$ and R are the velocity and the radius of the boundary. In this case, however, the mass M of the gas is constant. Therefore, we assume that the velocity distribution has the form

$$u = u_0 + (\dot{R} - u_0) r / R, \qquad u_0 = \alpha \dot{R} \quad (\alpha < 1). \tag{1}$$

Substitution of (1) into the continuity equation,

$$\frac{\partial \rho}{\partial t} + \frac{1}{r^2} \frac{\partial}{\partial r} (r^2 \rho u) = 0 \tag{2}$$

yields the following equation for the density $\rho(r, t)$:

$$\rho(r, t) = \rho_0(t) \tilde{\rho}(\xi), \qquad \xi = r / R; \tag{3}$$

$$\dot{\rho}_0 + \frac{3\dot{R}}{R}\rho_0 = \frac{u_0\rho_0}{R}\left(3 - \frac{2}{\xi} + \frac{\xi\tilde{\rho}'}{\tilde{\rho}} - \frac{\tilde{\rho}'}{\tilde{\rho}}\right), \quad \frac{d\rho}{d\xi} = \tilde{\rho}'. \quad (4)$$

The left-hand part of (4) can be expressed in terms of mass flow $\dot{M}$ near r = 0:

$$\dot{M} = 2\pi\rho_0\tilde{\rho}(\xi)u_0r^2 \quad (r \to 0), \quad (5)$$

whereupon Eq. (4) has the solution

$$\tilde{\rho}(\xi) = (1-\xi)^{(1-\mu)/\mu}\xi^{-2}, \quad \mu = \int_0^1 \tilde{\rho}(\xi)\xi^2 d\xi, \quad (3')$$

where μ is any arbitrary number. As expected, the density $\rho(r, t)$ becomes infinite when $r \to 0$, which is the "location" of the solid target of infinite mass.

We let $\mu = 1/2$ and obtain from the equation of motion

$$\partial p / \partial r = -\rho(\dot{u} + u\,\partial u / \partial r) \quad (7)$$

the pressure

$$p(\xi, t) = R\rho_0(t)\left[(a-b)\ln\xi + (a-b\xi)\frac{1-\xi}{\xi}\right],$$

$$a = R^{-1}(\dot{u}_0R + u_0\dot{R} - u_0^2),$$

$$b = rR^{-1}(\ddot{R}R - \dot{u}_0R - u_0\dot{R} + u_0^2).$$

The total gas energy E is

$$E(t) = \frac{2\pi}{\varkappa - 1}\int_0^R p(r, t)r^2dr + \frac{2\pi}{2}\int_0^R \rho(r, t)u^2r^2dr$$

$$= {}^1/_{12}\pi\rho_0R^3(\ddot{R}R + \dot{R}^2 + \dot{u}_0R + 3\dot{R}u_0 + 2u_0^2), \quad (8)$$

where κ is an adiabatic index, assumed equal to 5/3.[1)] On the other hand,

$$E(t) = \int_0^t q(t)\,dt \equiv \bar{q}t, \quad 0 < t < \tau,$$

where q(t) is the laser power, $\bar{q}$ is the average power, and τ is the pulse length.

Equations (4) and (5) yield the following equation for mass:

$$\dot{M} / M = 2u_0 / R = 2\alpha\dot{R} / R, \quad (9)$$

$$M = AR^{2\alpha}. \quad (10)$$

[1)]Allowance for ionization yields κ as a function of gas density and temperature. Some average value of κ should be selected in this case.

The solution of (8) and (10) is sought in the form $R = Bt^{\beta}$ $(t < \tau)$. As a result we have

$$\bar{q} = {}^1/_4AB^{2\alpha+2}, \quad \beta = 3/2(\alpha+1), \quad 1 < \beta < 1.5. \quad (11)$$

The energy flux $\bar{q}_0$ to the center is determined by mass flow $\dot{M}$:

$$\bar{q}_0 = \dot{M}\frac{u_0^2}{2} = \left[\frac{3\alpha}{2(\alpha+1)}\right]^3 AB^{2\alpha+2}. \quad (12)$$

A complete solution of the problem requires that the equation for the flux $\bar{q} - \bar{q}_0$ absorbed in the gas, a function of M and R, be added to (11) and (12). Since this relationship is unknown, it would be desirable to obtain such an equation from experimental data.

MOTION OF ZERO-CHARGE SURFACE AND ELECTRON EMISSION

The experiment recorded the charged-particle flow to a shielded probe. The experimental setup is shown in Fig. 1. A neodymium-glass laser was used as the source of the giant pulse. The oscillator comprised two rods 120 mm long and 12 mm in diameter, and the amplifier consisted of one rod. The Q-switch was actuated by a positive pulse with an amplitude of 35 kV supplied to a Kerr cell containing nitrobenzene. Such a laser was described in[14].

The laser beam was focused on the surface of carbon target 9 by lens 1 of 60 mm focal length. A portion of the beam was deflected by plane-parallel plates to coaxial photocell 10 and to a calorimeter to monitor the pulse shape and energy. Another portion of the beam was split off by a plane-parallel plate to be focused by lens 3 on spark gap 4. The breakdown in the spark gap was timed to coincide with the beginning of the laser pulse. The pulse formed in the spark gap proceeded across capacitance 5 simultaneously with the probe pulse to the

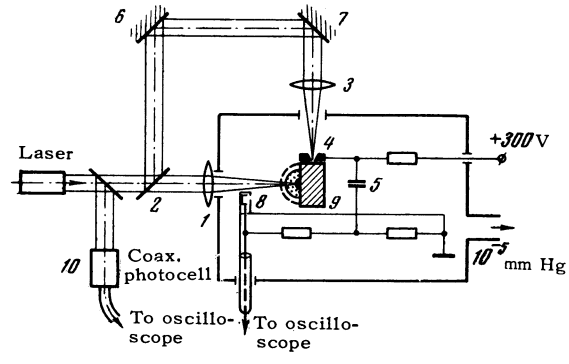

FIG. 1. Experimental setup for plotting the R-t diagram of the neutral boundary (see text for designations).

oscilloscope to provide the zero time mark minus the time lag of the deflection path 6, 7, 3. The upper limit of the time delay Δt of the spark gap breakdown can be computed from the maximum flare decay rate: $\Delta t \approx d/v \approx 10^{-9}$ sec. Here, $d \approx 0.01$ cm is the interelectrode distance, and the fast ion velocity at the edge of plasma is $v \approx 10^7$ cm/sec. The breakdown time was actually less than the computed value because the breakdown was determined by the plasma electrons. The signal from probe 8 was fed to the oscilloscope plates along a long coaxial cable. The zero-mark delay time was 4 nsec.

The expanding heated flare emitted electrons creating a negative space charge near the flare surface. The space charge in turn caused an excess of positive charge in the conductive plasma of the flare. A probe placed in the path of the expanding plasma is exposed first to the negative space charge and then to the positively charged conductive portion of the plasma. Since the amplitude of the probe signal recording the particle flow is proportional to the charge density, the passage of the negative space charge through the probe induces a negative voltage in the probe. The passage of the conductive plasma through the probe reverses the polarity of the signal. Consequently, the neighborhood of the flare edge contains a zero-charge surface whose motion can be recorded by the probe method when zero voltage appears at the probe. The location of the zero-charge surface can be determined quite accurately in spite of the fact that the width of the region marking the changeover from the negative space charge to the positive plasma charge is comparable to the flare dimensions.

The probe was a shielded Faraday cylinder covered with a metallic micron mesh at the end facing the target; it was 1 mm in size. The probe was matched to the coaxial lead to the vacuum chamber and to the transmitter cable. The resolving power of the sensing system, including the probe, was not worse than 2 nsec. Figure 2a shows a typical oscilloscope trace from the probe. The time marks are spaced 10 nsec apart. The zero time mark is visible at the beginning of the probe pulse. Figure 2b shows the laser emission pulse.

Carbon target 9 was placed in vacuum. Each laser pulse was focused on a different region of the target to secure similar initial conditions. In the experiment, the time delay t of the occurrence of a zero probe potential was measured as a function of the flight path R_0 to the probe. R − t diagrams were plotted for various values of the energy, which were controlled by neutral filters

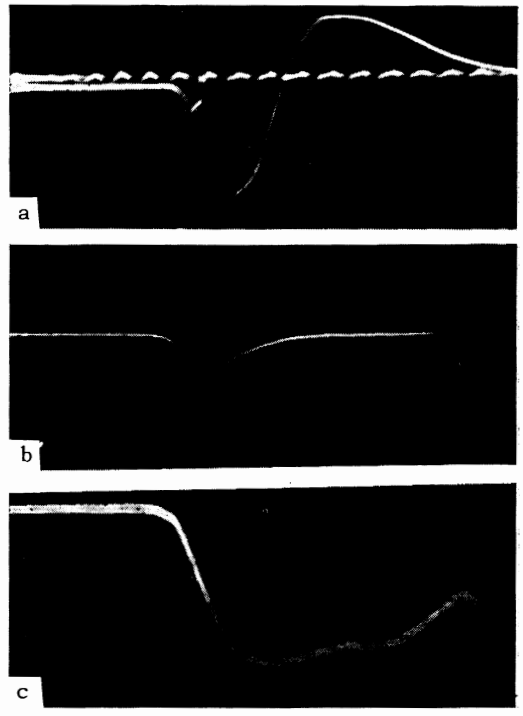

FIG. 2. Oscilloscopic traces: (a) probe signal, (b) laser emission pulse, (c) electron emission current.

calibrated in the laser beam. Figure 3b shows R − t diagrams of the motion of the zero-charge surface plotted for various powers. Curves 1 to 6 correspond to peak powers of 200, 51, 22, 5.6, 1.8, and 0.4 megawatts respectively. It is apparent that the velocity of the outward motion approaches asymptotically the value at the end of the pulse.

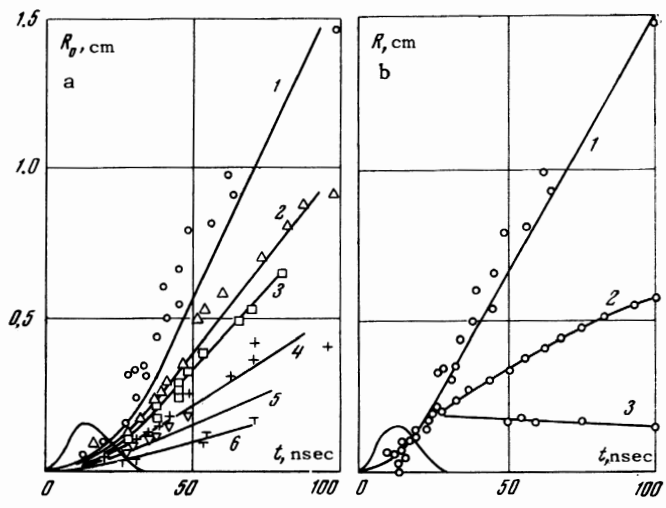

FIG. 3. R-t diagrams: (a) neutral boundary for various power values, (b) neutral boundary (curve 1), luminous edge (curve 2), and opaque region boundary (curve 3). Power output, 200 megawatts.

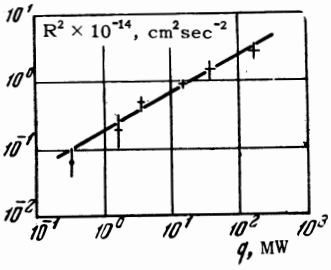

FIG. 4. Squared velocity of the neutral boundary as a function of power.

Figure 4 shows the squared velocity as a function of power. The errors are given with reference to maximum deviation. The plot is approximated by a straight line of slope $\gamma = 0.3$—0.6, which represents a power dependence of the boundary radius of the type $R \sim q^{\delta}$, where $\delta = 0.15$—0.3. A similar dependence was observed in the case of aluminum.

The ion velocity at the boundary, equal to 1.6×10^7 cm/sec, corresponds to an energy of 1.6 keV. It is difficult, however, to determine the plasma temperature from this velocity. The energy spectrum of these ions may also be strongly distorted by the collective interaction of the electron space charge with the boundary ions.[15]

The ion and electron density near the zero-charge surface can be determined from the emission current and energy distribution of the electrons. The electron emission current was measured with a spherical probe capable of intercepting practically all the emitted electrons. The probe was shielded by suppressor and grounded grids to eliminate the effects of secondary electron emission. Consequently, the probe measured the current of electrons whose energy exceeded a given value. A typical oscilloscope trace of the electron emission current from an expanding plasma is shown in Fig. 2c. The emission grows during the pulse, and then gradually decreases. According to curve 1 in Fig. 3a, at $t \approx 100$ nsec the zero-charge surface radius increases approximately 6 times relative to its value R_1 at the end of the laser pulse; the surface area of plasma enclosed in this boundary increases 36 times. Assuming that the emission is of thermal nature and comes from the surface, the emission current i is proportional to $R^2 n_e \langle v_e \rangle$, where the electron density is $n_e \sim R^{-3}$ and the mean electron velocity is $\langle v_e \rangle \sim T^{1/2}$. In the case of adiabatic expansion, $T \sim R^{-2}$, whence $i \sim R^{-2}$. The experiment, however, shows a weaker dependence on the radius, indicating non-equilibrium emission.

The emission current of electrons with energy ≥ 100 eV amounts to ~ 20 A. The time during which the emission decreases by one-half is 2×10^{-7} sec, which is much longer than the pulse. The total number of emitted electrons is $\sim 3 \times 10^{13}$. It is clear that electrons remove a negligible portion of the total plasma energy in a time interval comparable to the pulse length. The electron density in the space charge near the zero-charge surface can be obtained from the formula

$$n_e = i / 2\pi R^2 e \langle v_e \rangle,$$
$$\langle v_e \rangle = (2w_e / m_e)^{1/2},$$

where e, m_e, and w_e are the charge, mass, and energy of the electrons, respectively. It is assumed that the electron current is spherically symmetric, or else n_e denotes density averaged over the surface of zero charge. When $i \approx 20$ A, $w_e = 100$ eV, and $R_0 = R_1 = 0.25$ cm, the density is $n_e \approx 5 \times 10^{11}$ cm^{-3}. As can be seen from the oscilloscope trace shown in Fig. 2a, the ion current to the probe is comparable to the electron current on this surface. Consequently, the order of magnitude of the ion density at the flare boundary, given an ion velocity $\langle v_i \rangle \approx \langle v_e \rangle (m_e/m_i)^{1/2}$, will be $n_i \approx n_e (m_i/m_e)^{1/2}$ (where n_i and m_i are density and mass of the ions) or $n_i \approx 6 \times 10^{13}$ cm^{-3} (single ionization).

An analysis of the energy spectrum of the electrons by the retarded potential method shows that the average electron energy at the end of the pulse equals about 100 eV. The high value of energy of the emitted electrons indicates the presence of a considerable number of fast electrons in the flare.

DECAY OF LUMINOUS BOUNDARY

The motion of the luminous boundary was investigated with the aid of a high-speed camera, based on the SFR-2M type and operating as a photorecorder with a time resolution of 1.5 nsec. This resolution was due to increased slit image velocity relative to film, obtained by increasing mirror-to-film distance to 1.25 m. In addition, the RO-2M lens was replaced by a longer focus lens mounted outside the camera. The mirror speed was forced up to 90,000 rpm. A spectral slit 5 microns wide was used. Owing to the large diameter of the input lens, the space-time resolution was limited by mirror diffraction. Resolution was measured dynamically with the optical system operating as an autocollimator. The film was placed in a special corsette for processing to avoid deformation.

The flare was focused on the slit so as to render the slit parallel to the target surface at a slit-to-target distance of 0.4 mm. In the time scan, the beginning of slit luminescence lags behind the beginning of the flare decay by ~ 5 nsec. A typical recording of the transverse flare decay is shown in

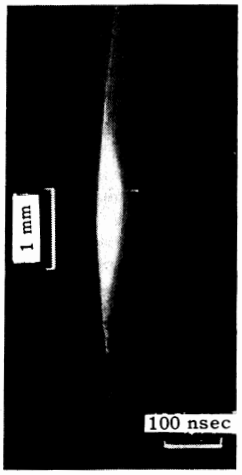

FIG. 5. Record of flare decay.

Fig. 5. A dense bright nucleus is visible in the center. Plasma continues to glow for a time after the passage of the pulse and practically disappears after 50 nsec. The velocity of the luminous edge at the termination of the pulse is 6.3×10^6 cm/sec (corresponding to an ion energy of 250 eV).

The motion of the luminous boundary is slowed down slightly with time by the rarefaction of plasma. The plasma density in the luminous boundary region in late decay stages (40 – 100 nsec), as determined by the twin probe saturation current in a transverse magnetic field, amounts to $10^{16} - 10^{17}$ cm^{-3}. Photographs were taken with various exposures differing by more than an order of magnitude. The measured velocity, however, was practically unchanged. This means that the luminous edge is quite sharp on the low density side. The R-t diagram of the luminous boundary is given in Fig. 3b (curve 2).

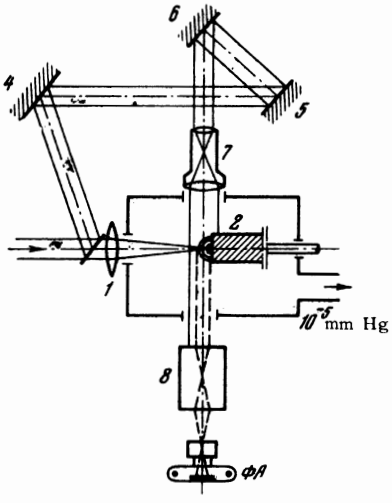

FIG. 6. Setup of the shadow method (see text for designations).

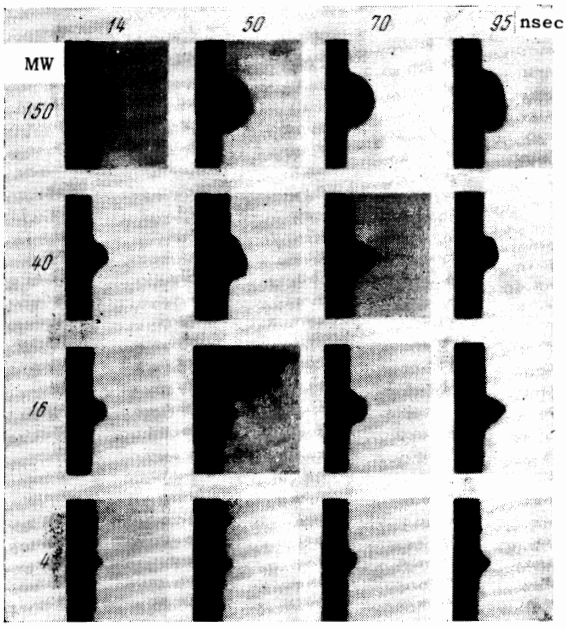

FIG. 7. Typical shadowgraph frames.

MOTION OF THE OPAQUE REGION

Owing to the nonuniform flare structure, a shadow method with laser pulse illumination was used to observe the motion of the internal region. The frame exposure was equal to the pulse length (see Fig. 2b). The main and back-illuminating pulses were synchronized by an optical delay path. Each frame was illuminated by a separate flash.

The experimental setup is shown in Fig. 6. The laser beam was focused by lens 1 on target 2. A portion of the beam was deflected into optical delay path 4—6. The beam was collimated by telescopic system 7. The shadow image was formed on photocathode 8 (electron-optical converter). The time delay was reckoned from the beginning of the main pulse to the middle of the back-illuminating pulse. The experimental method was otherwise similar to that used in the study of the neutral-front motion.

Figure 7 shows a number of frames of the flare shadowgraphs; numbers along the horizontal denote time delay, numbers along the vertical denote power, and frame field dimension along the horizontal is 7.5 mm. It is apparent that the flare has spherical symmetry, at least in the dense central region. The absorption edge is sharp and the diffraction structure is visible in some frames.

The R – t diagrams of the opaque region are given in Fig. 8, where curves 1, 2, and 3 correspond to 150, 40, and 4 megawatts respectively. When the power exceeds 40 megawatts, the shadow

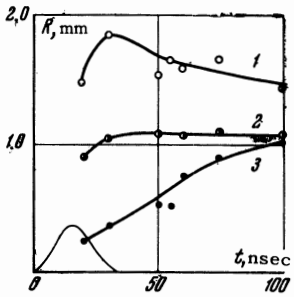

FIG. 8. R-t diagrams of the opaque region boundary for various laser output powers.

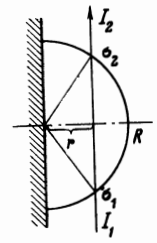

FIG. 9. Diagram to determine flare absorption.

boundary ceases its outward motion at the end of the pulse and slowly collapses towards the center. When the power is less than 30 megawatts, the opaque region appears and begins expanding after the end of the emission pulse, the expansion continuing during the first 100 nsec. According to the R − t diagram, the average velocity of the opaque region is fairly high in the presence of the pulse and reaches $\sim 6 \times 10^6$ cm/sec (see Fig. 8, curve 1).

The boundary of the opaque region appears to be close to the region of critical electron density n_0. The density is related to frequency by

$$n_0 = \pi \nu^2 m_e / e^2. \tag{13}$$

In the case of the neodymium laser ($\nu = 2.8 \times 10^{14}$ sec^{-1}), density $n_0 \approx 10^{21}$ cm^{-3}, and the ion density is of the same order of magnitude. It is also possible that the opaque region boundary has a high absorption coefficient, resulting in approximately the same value of density.

MEASUREMENT OF THE TRANSMISSION COEFFICIENT

Direct measurement of the absorption coefficient is difficult in various regions of the flare. Therefore, measurements were made to determine the transmission coefficient $\psi = \ln (I_1/I_2)$ near the boundary of the opaque region. The flare was probed with a narrow beam in the transverse direction. The measurement setup was analogous to that of shadow photography (Fig. 6), except that telescopic system 7 and electron-optical converter 8 were replaced by two confocal lenses of focal length 21 cm. The probing beam passed through the flare along the chord $\sigma_1\sigma_2$ (see Fig. 9). It was found that ψ has a large gradient near the opaque region, a fact readily apparent in the shadowgraphs. According to the measurements, $\partial\psi/\partial r \approx 100$ cm^{-1} at a distance of 0.4 mm from the opaque region. Although the nature of this gradient is not clear, it does not contradict the assumption that the absorption is due to the plasma. Furthermore, considering that the opacity of plasma is determined by absorption, the results of the measurements can be used to determine the coefficient of absorption which is found to be 20 cm^{-1} at a distance of $r \approx 2$ mm at the end of the pulse (at 150 megawatts).

DENSITY DISTRIBUTION IN THE FLARE

The plasma is heated and its motion is accelerated during the passage of the pulse. At high power, the motion is the same in all measured regions within the limits of experimental accuracy, because of the high plasma density. For comparison, Fig. 3b shows R − t diagrams of the motion of the zero-charge surface (curve 1), the luminous boundary (curve 2), and the absorption region (curve 3); it is apparent that curves 1 and 2 trace similar courses after the end of the pulse. This indicates to some extent that the density distribution in the flare may have the form of expression (3). The estimated values of density in various regions of the flare reveal large gradients in the density distribution as $r \to 0$, in qualitative agreement with (3′). The temperature of the flare region near the luminous boundary 70 nsec after the end of the pulse was determined from the electron conductivity in a transverse magnetic field to be about 5000°. In order of magnitude, this temperature is in agreement with experiments involving luminescence of metal vapor emitted by a shock wave emerging from the free surface of a metal.[16,17]

The diagram in Fig. 10 shows the density distribution in the flare at the end of a 150-MW pulse. The dense central nucleus bounded by sphere 1 with a radius r = 0.16 cm has a density $\geq 10^{21}$ cm^{-3}. The density decreases from $\sim 10^{21}$ to $\sim 10^{18}$ cm^{-3} in region 2 with $0.16 \leq r \leq 0.18$ cm. In region 3, with $0.18 \leq r \leq 0.25$ cm, the density drops to $\sim 4 \times 10^{13}$ cm^{-3}. Region 4 is an electron space charge with density $\sim 5 \times 10^{11}$ cm^{-3} near $r \approx 0.25$ cm. At a later time, 70 nsec after the end of the pulse, the density distribution has the follow-

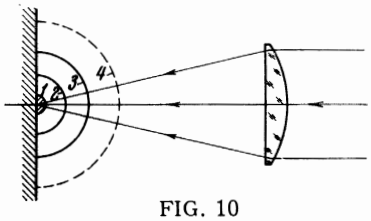

FIG. 10

ing pattern: the radius of region 1 of density $\geq 10^{21}$ cm^{-3} equals 0.14 cm; the outer radius of region 2 of density $\sim 10^{16}$ cm^{-3} is 0.6 cm; and in region 3, with $0.6 \leq r \leq 1.6$ cm, the density drops from 10^{16} to 10^{12} cm^{-3}.

It may be also noted that the decaying flare emits electrons whose current reaches tens of amperes. These currents should induce a magnetic field which may affect the angular distribution of the emitted particles. The magnitude of the magnetic field corresponding to these currents amounts to tens of oersteds.

Let us determine the volume-averaged temperature T in the flare at the end of the pulse. As noted at the beginning of this paper, the special feature of the heating process under consideration is the increase in mass of the heated gas that takes place during the passage of the pulse. Since in the course of heating the gas dynamic energy E_g and the thermal energy E_t are comparable, $E_t \sim E$ in the order of magnitude, i.e., $TM \sim E$ (it is assumed here that heat capacity is constant and ionization does not introduce qualitative changes). It follows that the lower the heated (i.e., "vaporized") mass the higher the temperature, whereas a constant mass has $T \sim E$.[1] Therefore, due allowance for the change in gas mass that takes place during the passage of the pulse is basic in our case. The relationship between T and M is determined by the absorption of radiation by the heated gas. In a qualitative sense it is clear that the higher the coefficient of absorption in the gas the higher the temperature reached at the end of the pulse and the smaller the vaporized mass.

As noted above, for a complete theoretical analysis of the flare motion we lack an equation for the absorption of radiation by the gas. This equation can be replaced by a relationship obtained from experimental data, such as the flare radius R_1 at the end of the emission pulse as a function of power (see Fig. 3a):

$$R_1 = 0.13\,\bar{q}^{0.15}, \tag{14}$$

where q is in megawatts. The vaporized mass M is related to the energy and to the radius R_1, according to (11), by

$$\tau^2 E = {}^1/_4 M_1 R_1^2, \tag{15}$$

When E = 3 J, τ = 30 nsec, and R_1 = 0.25 cm ($\bar{q}$ = 100 MW), the heated mass of gas amounts to $M_1 \sim 2 \times 10^{-6}$ g. According to (8), the thermal energy E_t equals 0.31 E which yields 56 eV per atom. Allowing for double ionization, the average temperature is ~7 eV, and the maximum temperature is approximately 2.5 times the average value.

The above estimates were based on the assumption of an ideal gas with an adiabatic index $\kappa = 5/3$. It is readily apparent that an allowance for ionization changes the relationship between the specific internal energy ϵ and the pressure p, so that for a given p, ϵ increases at the expense of the ionization energy, i.e., the value of κ in the expression $\epsilon = p/\rho(\kappa - 1)$ decreases. It follows from (8) that the ratio of internal to total energy of the gas increases in this case.

In conclusion, let us make a few remarks about the late stages of flare decay. After the end of the pulse, the gas motion becomes adiabatic with constant mass M_1, and the gas temperature decreases with time. It should be noted, however, that in the heating process the gas had an initial velocity u_0 at the point r = 0. As a result, the heated gas leaves the target surface and its mass is distributed in the expanding spherical layer. Therefore, the gas density in the late decay stages should pass through a maximum within region 2 (Fig. 10) near its upper boundary. This is confirmed, in particular, in the recording shown in Fig. 5.

It seems to us that the appearance of the opaque region can be related to the ejection of matter of comparatively low temperature, due to thermal conductivity in the plasma-solid transition layer, or, what seems to be more probable, due to the discharge of dense material compressed by a pressure pulse on the order of $E/R^3 \approx 10^{10}$ dynes/cm^2 and comparable to $\rho^0 c^2$ (ρ^0 and c are the density and sound velocity in the solid).

The results of the experimental data thus seem to be in agreement with the theoretical interpretation of the heating and motion of the flare given in this paper.

The authors are grateful to V. S. Zuev for his collaboration in the experiments.

[1] N. G. Basov and O. N. Krokhin, JETP 46, 171 (1964), Soviet Phys. JETP 19, 123 (1964).

[2] O. N. Krokhin, ZhTF 34, 1324 (1964), Soviet Phys. Tech. Phys. 9, 1024 (1965).

[3] N. G. Basov and O. N. Krokhin, Proc. of the Conf. on Quantum Electronics, Paris, 1963.

[4] J. M. Dauson, Phys. Fluids 7, 981 (1964).

[5] A. F. Haught and D. H. Polk, Conference on

Plasma Physics and Controlled Nuclear Fusion Research, Culham, 1965, Report CN-21/110.

[6] W. I. Linlor, Appl. Phys. Lett. 3, 210 (1963).

[7] W. I. Linlor, Phys. Rev. Lett. 12, 383 (1964).

[8] U. Ascoli-Bartoli, C. De Michelis, and E. Mazzucato, Conf. on Plasma Physics and Controlled Nuclear Fusion Research, Culham, 1965, Report CN-21/77.

[9] O. E. Bodgankevich, V. Yu. Sudzilovskiĭ, and A. A. Lozhnikov, ZhTF 35, 2052 (1965), Soviet Phys. Tech. Phys. 10, 1573 (1966).

[10] H. Opower and E. Burlefinger, Phys. Lett. 16, 37 (1965).

[11] R. V. Ambartsumyan, N. G. Basov, B. A. Bouko, V. S. Zuev, O. N. Krokhin, P. G. Kryukov, Yu. V. Senat-skiĭ, and Yu. Yu. Stoĭlov, JETP 48, 1583 (1965), Soviet Phys. JETP 21, 1061 (1965).

[12] I. V. Nemchinov, PMTF No. 5, 18 (1964).

[13] L. I. Sedov, Metody podobiya i razmernosti v mekhanike (Methods of Similarity and Dimensionality in Mechanics), Gostekhizdat, 1957.

[14] N. G. Basov, V. S. Zuev, and Yu. V. Senat-skiĭ, JETP Letters 2, 57 (1965), transl. p. 35.

[15] A. V. Gurevich, L. V. Pariĭskaya, and L. P. Pitaevskiĭ, JETP 49, 8 (1965), Soviet Phys. JETP 22, 4 (1966).

[16] S. B. Kormer, M. V. Sinitsyn, and A. I. Kuryapin, In: Ya. B. Zel'dovich and Yu. P. Raĭzer, Fizika udarnykh voln i vysokotemperaturnykh gidrodinamicheskikh yavleniĭ (Physics of Shock Waves and High-temperature Hydrodynamic Phenomena), Nauka, 1966, pp. 601-605.

[17] Ya. B. Zel'dovich and Yu. P. Raĭzer, JETP 35, 1402 (1958), Soviet Phys. JETP 8, 980 (1959).

Translated by S. Kassel
116